A simplified approach for computed tomography with an X-ray grating interferometer

P. C. Diemoz,[1,2,*] P. Coan,[1,2,3] I. Zanette,[1] A. Bravin,[1,2] S. Lang,[5] C. Glaser,[2,4] and T. Weitkamp[1,6]

[1] *European Synchrotron Radiation Facility (ESRF), 6 rue Horowitz, 38043 Grenoble, France*
[2] *Munich-Centre for Advanced Photonics, Ludwig-Maximilians University (LMU), Munich, Germany*
[3] *Faculty of Medicine, Ludwig-Maximilians University (LMU), Marchioninistrasse 15, 81377 Munich, Germany*
[4] *Institut fur Klinische Radiologie, Ludwig-Maximilians University (LMU), Marchioninistrasse 15, 81377 Munich, Germany*
[5] *Biomaterials Science Center, University of Basel, Schanzenstrasse 46, 4031 Basel, Switzerland*
[6] *Synchrotron Soleil, L'Orme des Merisiers, Saint-Aubin, 91192 Gif-sur-Yvette, France*
**diemoz@esrf.fr*

Abstract: We present a simplified acquisition and processing method for X-ray grating interferometry computed tomography (CT). The proposed approach eliminates the need to scan the gratings, thus allowing for a faster CT acquisition compared to methods presently in use. The contrast in the reconstructed images can be expressed as a linear combination of the absorption and refraction within the sample. Experimental images of a test phantom made of known materials and a human bone-cartilage sample prove the correctness of the method and show very good agreement with the theory. The here proposed approach might be highly interesting in many fields where a reduced imaging acquisition time is requested and/or where the radiation dose delivered to the sample has to be kept low, such as, for example, in in-vivo imaging.

OCIS codes: (110.6955) Tomographic imaging; (110.7440) X-ray imaging; (050.1950) Diffraction gratings.

References and links

1. C. David, B. Nöhammer, H. H. Solak, and E. Ziegler, "Differential X-ray phase contrast imaging using a shearing interferometer," Appl. Phys. Lett. **81**(17), 3287–3289 (2002).
2. R. Fitzgerald, "Phase sensitive X-ray imaging," Phys. Today **53**(7), 23 (2000).
3. A. Momose, T. Takeda, Y. Itai, and K. Hirano, "Phase-contrast X-ray computed tomography for observing biological soft tissues," Nat. Med. **2**(4), 473–475 (1996).
4. P. Cloetens, W. Ludwig, J. Baruchel, D. Van Dyck, J. Van Landuyt, J. P. Guigay, and M. Schlenker, "Holotomography: Quantitative phase tomography with micrometer resolution using hard synchrotron radiation x rays," Appl. Phys. Lett. **75**(19), 2912–2914 (1999).
5. D. Chapman, W. Thomlinson, R. E. Johnston, D. Washburn, E. Pisano, N. Gmür, Z. Zhong, R. H. Menk, F. Arfelli, and D. Sayers, "Diffraction enhanced x-ray imaging," Phys. Med. Biol. **42**(11), 2015–2025 (1997).
6. A. Bravin, "Exploiting the X-ray refraction contrast with an analyser: the state of the art," J. Phys. D Appl. Phys. **36**(10A), A24–A29 (2003).
7. J. Keyriläinen, M. Fernández, M. L. Karjalainen-Lindsberg, P. Virkkunen, M. Leidenius, K. von Smitten, P. Sipilä, S. Fiedler, H. Suhonen, P. Suortti, and A. Bravin, "Toward high-contrast breast CT at low radiation dose," Radiology **249**(1), 321–327 (2008).
8. A. Olivo, and R. Speller, "Image formation principles in coded-aperture based x-ray phase contrast imaging," Phys. Med. Biol. **53**(22), 6461–6474 (2008).
9. A. Momose, S. Kawamoto, I. Koyama, Y. Hamaishi, K. Takai, and Y. Suzuki, "Demonstration of X-Ray Talbot interferometry," Jpn. J. Appl. Phys. **42**(Part 2, No. 7B), L866–L868 (2003).
10. T. Weitkamp, A. Diaz, C. David, F. Pfeiffer, M. Stampanoni, P. Cloetens, and E. Ziegler, "X-ray phase imaging with a grating interferometer," Opt. Express **13**(16), 6296–6304 (2005).
11. S. A. McDonald, F. Marone, C. Hintermüller, G. Mikuljan, C. David, F. Pfeiffer, and M. Stampanoni, "Advanced phase-contrast imaging using a grating interferometer," J. Synchrotron Radiat. **4**, 562–572 (2009).
12. F. Pfeiffer, T. Weitkamp, O. Bunk, and C. David, "Phase retrieval and differential phase-contrast imaging with low-brilliance X-ray sources," Nat. Phys. **2**(4), 258–261 (2006).

#135564 - $15.00 USD Received 23 Sep 2010; revised 26 Oct 2010; accepted 27 Oct 2010; published 14 Jan 2011

13. A. Momose, W. Yashiro, H. Maikusa, and Y. Takeda, "High-speed X-ray phase imaging and X-ray phase tomography with Talbot interferometer and white synchrotron radiation," Opt. Express **17**(15), 12540–12545 (2009).
14. H. Wen, E. E. Bennett, M. M. Hegedus, and S. Rapacchi, "Fourier X-ray scattering radiography yields bone structural information," Radiology **251**(3), 910–918 (2009).
15. M. Born, and E. Wolf, *Principles of optics: electromagnetic theory of propagation, interference and diffraction of light* (Cambridge University Press, Cambridge,1999).
16. F. Pfeiffer, M. Bech, O. Bunk, P. Kraft, E. F. Eikenberry, Ch. Brönnimann, C. Grünzweig, and C. David, "Hard-X-ray dark-field imaging using a grating interferometer," Nat. Mater. **7**(2), 134–137 (2008).
17. T. Weitkamp, P. Tafforeau, E. Boller, P. Cloetens, J. P. Valade, P. Bernard, F. Peyrin, W. Ludwig, L. Helfen, and J. Baruchel, "Status and evolution of the ESRF beamline ID19," in *X-Ray Optics and Microanalysis, Proceedings*, M. A. Denecke and C. T. Walker, eds. (Amer Inst. Physics, Melville), pp. 33–38.
18. T. Weitkamp, I. Zanette, C. David, J. Baruchel, M. Bech, P. Bernard, H. Deyhle, T. Donath, J. Kenntner, S. Lang, J. Mohr, B. Müller, F. Pfeiffer, E. Reznikova, S. Rutishauser, G. Schulz, A. Tapfer, and J. Valade, "Recent developments in X-ray Talbot interferometry at ESRF-ID19," Proc. SPIE **7804**, 780406 (2010).
19. P. Coan, A. Peterzol, S. Fiedler, C. Ponchut, J. C. Labiche, and A. Bravin, "Evaluation of imaging performance of a taper optics CCD; FReLoN' camera designed for medical imaging," J. Synchrotron Radiat. **3**, 260–270 (2006).
20. P. Coan, F. Bamberg, P. C. Diemoz, A. Bravin, K. Timpert, E. Mützel, J. G. Raya, S. Adam-Neumair, M. F. Reiser, and C. Glaser, "Characterization of osteoarthritic and normal human patella cartilage by computed tomography X-ray phase-contrast imaging: a feasibility study," Invest. Radiol. **45**(7), 437–444 (2010).
21. P. C. Diemoz, A. Bravin, C. Glaser, and P. Coan, "Comparison of analyzer-based imaging computed tomography extraction algorithms and application to bone-cartilage imaging," Phys. Med. Biol. (to be published).

1. Introduction

X-ray grating interferometry (XGI) is a phase-contrast imaging technique that exploits, for generating the image contrast, diffraction from a grating used in combination with a highly spatially coherent X-ray beam and absorption in a second grating used as an analyzer [1]. Like other phase-contrast imaging methods that have been proposed and applied in the recent years [2–8], in XGI the image formation does not rely only on the X-ray absorption effect but also on the phase shift induced by the object onto the incoming beam. Therefore, it has been shown that it has the potential for much increased image contrast if compared to conventional absorption-based X-ray imaging of low absorbing materials, like the ones encountered in biological tissues. XGI in both projection and Computed Tomography (CT) modes is now used at different third generation synchrotron facilities [9–11]. Moreover, it was shown that XGI can also be applied with sources delivering spatially incoherent radiation, like commercially available X-ray tubes, by using a third grating placed just downstream of the source [12]. XGI has therefore the potential to find wide application in various fields, and especially in medical imaging where an increased image contrast can facilitate the diagnosis. In the "phase stepping" technique usually applied for data acquisition in grating interferometry [10], the scanning of one grating and the acquisition of several images, one for each step of the grating scan, are required. When CT imaging is performed, this procedure has to be repeated for each viewing angle, which leads to a high number of collected images, long integral acquisition time and considerable dose delivered to the sample. Other methods, which do not require scanning of the gratings, exist [13,14], but have the disadvantage of a much reduced spatial resolution. In this article, we propose a method that enables to simplify the acquisition by requiring only a single image per projection angle.

In a grating interferometer, the two gratings are positioned at a mutual distance such that the self-imaging effect of the first grating (G_1) occurs at the position of the second grating (G_2) [9]. G_1 is made of an array of phase shifting lines, while G_2 consists of an array of absorbing lines with the same periodicity and orientation of the fringes induced by G_1. If the phase stepping method is adopted and one of the two gratings is shifted in the direction normal to both the optical axis and the gratings lines, the intensity in each pixel will oscillate as a function of grating position. In many cases the oscillation can be approximated as a sinusoid as represented in Fig. 1(b) [10]. If an object is placed in the X-ray beam, the emerging refracted X-rays will locally shift the position of the fringes, absorption will lower

#135564 - $15.00 USD Received 23 Sep 2010; revised 26 Oct 2010; accepted 27 Oct 2010; published 14 Jan 2011

the average value and scattering will decrease the fringes visibility (*V*, defined as the relative difference between the peak and average intensities). This quantitative information can then be extracted mathematically. In CT mode, the rotation axis of the sample is usually oriented in the same direction of the gratings lines and the three-dimensional (3D) distributions of the absorption coefficient μ, of the refractive index decrement δ and of the amount of scattering are reconstructed using filtered-back projection (FBP) algorithm [12].

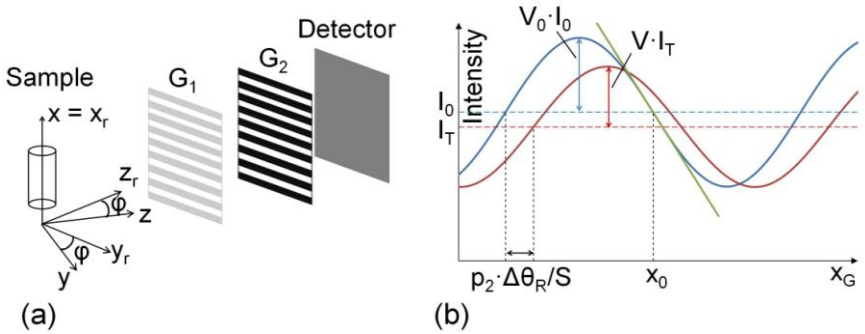

Fig. 1. (a) Scheme of the XGI setup used for this study, with gratings lines perpendicular to the sample rotation axis. (b) Sinusoidal fringe pattern measured with the phase stepping method, the linear approximation of the curve around the point x_0 is indicated. *V* represents the visibility, I_0 the intensity incident on the object and I_T the transmitted intensity.

2. Theory: a new reconstruction method

Let us consider, instead, the configuration shown in Fig. 1(a), in which G_1 and G_2 have the gratings lines oriented in the horizontal direction, and the rotation axis of the sample is vertical. The coordinate system (x,y_r,z_r) of both the X-ray beam and the detector is rotated with respect to the sample reference frame (x,y,z) by an angle φ around the CT axis *x*. The beam propagates along z_r and the gratings lines are parallel to y_r. In this geometry the gratings are therefore sensitive to the component of the refraction angle that is parallel to the *x* axis.

It can be shown [15] that the logarithm of the transmitted intensity I_T and the vertical component of the refraction angle $\Delta\theta_R$ can be expressed as line projections respectively of the linear attenuation coefficient (μ):

$$-\ln\left[I_T(x,y_r)/I_0(x,y_r)\right]=\int dz_r\,\mu(x,y_r,z_r), \tag{1}$$

and of the gradient of the refractive index decrement (δ):

$$\Delta\theta_R(x,y_r)=\int dz_r\,\frac{\partial\delta}{\partial x}(x,y_r,z_r). \tag{2}$$

Let us denote by T_{GR} the average intensity transmission through the gratings and by $S = p_2/d_{Talbot}$ (where p_2 is the period of G_2 and d_{Talbot} is the considered fractional Talbot distance) the angle corresponding to one grating period. If we indicate with $\psi(x,y_r)$ the shift of the sinusoidal fringe profile and with x_G the relative position of the two gratings, the beam intensity at each point of the detector is [16]:

$$I(x_G;x,y_r)=T_{GR}(x,y_r)I_T(x,y_r)\left[1+V(x,y_r)\sin\left(\psi(x,y_r)+\frac{2\pi}{p_2}x_G+\frac{2\pi}{S}\Delta\theta_R(x,y_r)\right)\right]= \tag{3}$$
$$=T_{GR}(x,y_r)I_T(x,y_r)G(x_G;\Delta\theta_R;x,y_r),$$

where $G(x_G;\Delta\theta_R;x,y_r)$ is a function of both the object and the imaging system.

#135564 - $15.00 USD Received 23 Sep 2010; revised 26 Oct 2010; accepted 27 Oct 2010; published 14 Jan 2011

We will assume here that the scattering introduced by the object is negligible, so that the visibility map $V(x,y_r)$ is the same when recorded with or without the object. It is worthwhile to note that $V(x,y_r)$ and $\psi(x,y_r)$ can be easily measured from phase stepping scans acquired before inserting the object in the beam. We will further assume that V and ψ are spatially homogeneous, so that their dependence on x and y_r can be neglected.

In analogy with conventional absorption CT, we consider the following quantity:

$$-\ln\frac{I(x,y_r)}{I_0(x,y_r)T_{GR}(x,y_r)}=\int dz_r\mu(x,y_r,z_r)-\ln\left[G(x_G;\Delta\theta_R)\right]. \tag{4}$$

The first term on the right side of Eq. (4) is the usual Radon transform encountered in conventional CT. Since this term has the form of a line integral, the values of $\mu(x,y,z)$ can be reconstructed by applying conventional algorithms like FBP. In the case of XGI there is an additional term depending on refraction. This term generally does not have the form of a line integral. However, if the working point x_G is chosen such that $\psi+2\pi x_G/p_2=n\pi$ (n = 0,1,2..), where $\ddot{G}=0$ and $\dot{G}$ is maximum (see point x_0 in Fig. 1(b)), and in the hypothesis that $\Delta\theta_R << S/4$, then we can apply the first-order Taylor expansion around $\Delta\theta_R = 0$:

$$\begin{aligned}&\ln\left[G(x_G;\Delta\theta_R)\right]\approx\ln\left[G(x_G;\Delta\theta_R=0)\right]+\frac{1}{G(x_G;\Delta\theta_R=0)}\dot{G}(x_G;\Delta\theta_R=0)\Delta\theta_R(x,y_r)=\\&=K_1(x_G)+K_2(x_G)\cdot\int dz_r\frac{\partial\delta}{\partial x}(x,y_r,z_r),\end{aligned} \tag{5}$$

where we have expressed $\Delta\theta_R$ as a function of δ and where the quantities $K_1(x_G)$ and $K_2(x_G)$ depend only on the chosen gratings position and are therefore constant in our case. By inserting Eq. (5) in Eq. (4) and applying the FBP algorithm, the following quantity can be reconstructed for each point of the object:

$$f(x,y,z)=\mu(x,y,z)-\frac{K_1(x_G)}{L}-K_2(x_G)\cdot\frac{\partial\delta}{\partial x}(x,y,z), \tag{6}$$

where L is the dimension of each angular projection image in the y_r direction, which determines the diameter of the reconstructed slice. The value calculated for each point of the object is therefore given by a linear combination of μ and of the vertical gradient of δ.

This expression was obtained under the assumption that scattering is negligible. However, if the scattering angles are sufficiently small, so that $\Delta\theta_R+\Delta\theta_{Scatt}<<S/4$, the approximation is still valid. If we consider the first order approximation of the function G, in fact, scattering positive and negative contributions cancel out.

The choice of the working point x_G in the linear region of the intensity function G presents two advantages. The first derivative $\dot{G}$ is maximized: this implies that the highest sensitivity to refraction can be achieved at this point since the coefficient K_2 in Eq. (6) is also maximized. Besides, since the second derivative $\ddot{G}$ is equal to zero, the interval of validity of the first-order Taylor approximation for G is relatively large. Other positions along the intensity function may be used, but this would inevitably lead to a reduction of the refraction sensitivity and to more stringent requirements on the values of the refraction angles introduced by the object.

3. Experimental methods

The experimental verification was carried out at the ID19 beamline [17] of the European Synchrotron Radiation Facility using a monochromatic X-ray beam ($\Delta E/E\approx10^{-4}$) of 32 keV. A silicon π-shifting grating (G_1), with period p_1 = 4.787 μm and thickness t_1 = 45 μm, and a

#135564 - $15.00 USD Received 23 Sep 2010; revised 26 Oct 2010; accepted 27 Oct 2010; published 14 Jan 2011

gold absorption grating (G_2) with period p_2 = 2.4 μm and thickness t_2 = 50 μm, were used, in the geometry of Fig. 1(a). The technical details of the interferometer setup are described elsewhere [18]. The distance between G_1 and G_2 was 37 cm (5th fractional Talbot distance for the energy used); the sample-to-detector distance was 55 cm. In these experimental conditions a visibility of 32% was obtained. The images were recorded by a FReLoN CCD camera [19] with 2048 x 2048 pixels coupled with a lens system to a scintillator. The effective pixel size of the detector was 8 μm.

The first sample, a phantom made of objects of known composition and geometry, consisted of two hollow polypropylene cylinders, with an outer diameter of 2.3 mm and a wall thickness of 0.4 mm, inclined by approximately 11° with respect to the vertical axis and containing, respectively, ethanol and a 10% formalin solution. The second sample was a bone-cartilage cylinder with a diameter of approximately 8 mm, extracted from a human patella. The specimen was placed in a cylindrical plastic container and dipped into a 10% formalin solution. CT scans of both samples were performed with the gratings kept fixed at a relative position x_0, as in Fig. 1(b). 800 angular projections over 360° were recorded for imaging the plastic phantom and 1600 for the bone-cartilage sample. For comparison, an additional phase stepping CT acquisition was carried out for the plastic phantom at three gratings positions over one period, with the same angular sampling and the same exposure time for each raw projection image as in the previous case. A 2x2 binning of the detector pixels was used for the scans of the plastic phantom, leading to an effective pixel size of 16 μm.

4. Results and discussion

3D distributions of absorption and refraction have been reconstructed for the test phantom by using the phase stepping method. The combined absorption-refraction (according to Eq. (6) has been obtained by directly applying the FBP algorithm to the angular projections acquired at one fixed position of the gratings. An example of the resulting absorption, refraction and combined CT images obtained for the same slice within the sample are reported respectively in Figs. 2(a)–2(c) for the cylinder containing ethanol and in Figs. 2(d)–2(f) for that containing the formalin solution.

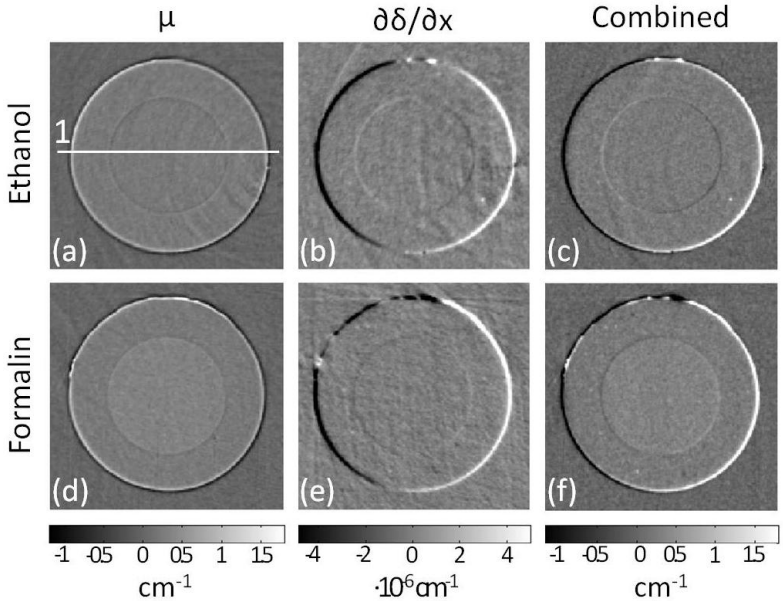

Fig. 2. Reconstructed axial slices for the two cylinders containing ethanol (a,b,c) and formalin (d,e,f): absorption (a,d) and refraction (b,e) images obtained with phase stepping method and combined absorption-refraction images (c,f) obtained for one fixed gratings position.

#135564 - $15.00 USD Received 23 Sep 2010; revised 26 Oct 2010; accepted 27 Oct 2010; published 14 Jan 2011

In the absorption images, the difference in intensity between the plastic cylinder and the liquid is more pronounced for formalin than for ethanol because the linear attenuation coefficients for the liquid and for the plastic container differ more in the first case (μ_{pol} = 0.23 cm^{-1}, μ_{form} = 0.35 cm^{-1}, μ_{eth} = 0.24 cm^{-1}). Edge enhancement due to propagation-based ("inline") phase contrast is also observable in the absorption images, due to the finite propagation distance between the sample and the detector [10]. In the refraction images a signal is produced at the interfaces between materials. It is interesting to remark that the black-white contrast is reversed for the polypropylene-formalin boundary (Fig. 2(e)) with respect to the polypropylene-ethanol boundary (Fig. 2(b)), because the difference in the δ values has opposite signs in the two cases ($\delta_{pol} = 2.0 \cdot 10^{-7}$, $\delta_{form} = 2.3 \cdot 10^{-7}$, $\delta_{eth} = 1.8 \cdot 10^{-7}$). In Figs. 2(c) and 2(f), as expected from the theory, the absorption and refraction signals visible in the previous images are combined in the same image and the variations of μ and δ can be qualitatively evaluated.

For a quantitative comparison, the profiles over a horizontal line across the cylinders in Figs. 2(a)–2(c) have been considered; the profiles for absorption, refraction and combined absorption-refraction signals are reported in Fig. 3(a). In Fig. 3(b) the profile for combined absorption-refraction is compared to that obtained using Eq. (6). The latter has been calculated using the absorption and refraction images reconstructed from the phase stepping method and the theoretical values for the coefficients (estimated in $K_1(x_0) \approx 0$ and $K_2(x_0) \approx -3.1 \cdot 10^5$ in our experimental conditions). An excellent agreement between the absorption and the combined absorption-refraction images in the regions where refraction is absent (i.e. far from the interfaces) is obtained (Fig. 3(a)). Furthermore, the combined absorption-refraction profile is very close to that expected from Eq. (6) (Fig. 3(b)), both in regions where absorption is the only signal and in regions where refraction is predominant, like at the boundaries between the different materials.

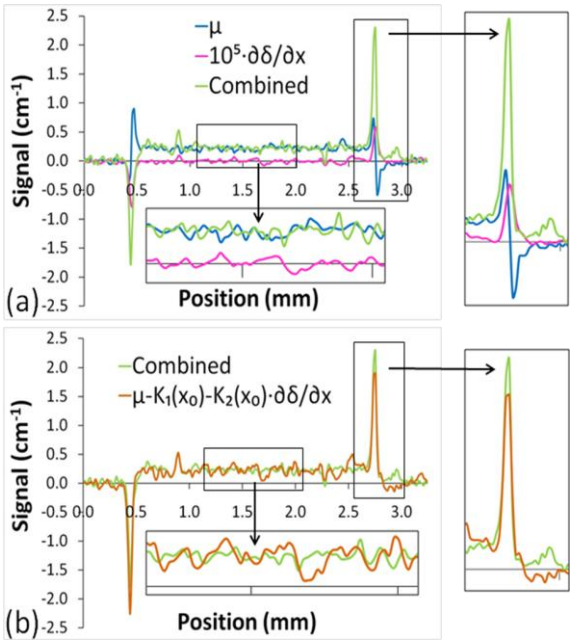

Fig. 3. Profiles across the cylinder containing ethanol (line 1 in Fig. 2(a)). In (a), absorption and refraction profiles extracted with phase stepping method are reported (the latter multiplied by 10^5 for visualization purposes), together with absorption-refraction combined profile obtained from a single gratings position. In (b), the absorption-refraction combined profile is compared to that theoretically expected from Eq. (6) (see text).

#135564 - $15.00 USD Received 23 Sep 2010; revised 26 Oct 2010; accepted 27 Oct 2010; published 14 Jan 2011

The signal-to-noise ratio (SNR) (defined as the ratio between the pixels average value and their standard deviation) has been calculated in regions of interest (ROI) within the different materials. SNR is about 1.51-1.68 times higher in the absorption image than in the combined image. This result is close to the expected value of $\sqrt{3} \approx 1.73$ that can be estimated considering that in the phase stepping acquisition the irradiation time was three times larger. To evaluate the statistical errors in the refraction signal, for each (negative and positive) refraction peak of the two cylinders, the area under the peak has been calculated for ten adjacent horizontal lines. The obtained SNR values (defined as the ratio between the average integral values over the ten lines and their standard deviation) are only 1.04 to 1.41 times higher in the refraction image than those for the combined image, despite of the much shorter exposure time in the latter case. This result suggests that the here presented method may be more robust to noise than the phase stepping method.

In Fig. 4(a) the bone-cartilage sample reconstructed from the CT acquisition with a fixed gratings position is presented; Fig. 4(b) is a zoom within the cartilage. Both the internal structure of the bone and the contours of the cartilage tissue are clearly identifiable on the top and bottom regions of Fig. 4(a), respectively. The signal in the bone is given by a combination of absorption of the bulk and of refraction at the edges of the trabecular meshwork. Concerning cartilage, the signal is mainly given by the refraction occurring at the boundaries between the tissue and the surrounding liquid. A closer inspection to the cartilage reveals also that small spherical structures are visible, which can identified as single cartilage cells (chondrocytes) or clusters of them (chondrons) [20]. Chondrons and chondrocytes show a reversed black-white contrast if compared to the cartilage-liquid interface, since they are characterized by a refractive index decrement lower than the surrounding cartilage matrix [21]. Note, however, that the energy of 32 keV used in these acquisitions is not optimized to reveal these details.

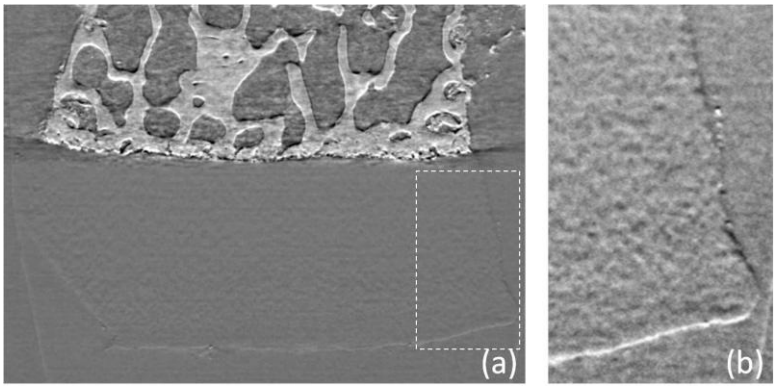

Fig. 4. Images of a human bone-cartilage sample calculated by using the combined absorption-refraction reconstruction: (a) reconstructed CT vertical plane of the bone and cartilage tissues (respectively at the top and bottom parts of the image), (b) expanded view of a cartilage tissue region.

5. Conclusions

We have proposed a simplified method for CT data acquisition and reconstruction in X-ray grating interferometry. This technique needs only one raw image per viewing angle and does not require any motion of the gratings, which can remain in a fixed position with respect to each other and the rest of the setup. The procedure does not allow obtaining separate maps of the absorption and refraction of the sample, respectively, but produces images in which the contrast is generated by a combination of the two effects. However, this mixed signal contains more information than the absorption or refraction image alone and, from a diagnostic point of view, it may be advantageous. Important benefits arise from the fact that this method

#135564 - $15.00 USD Received 23 Sep 2010; revised 26 Oct 2010; accepted 27 Oct 2010; published 14 Jan 2011

eliminates the need for moving the gratings during acquisition of a tomography scan. In particular, a greater stability of the setup can be obtained and also a reduction in the total acquisition time, because of the reduced number of image frames and the removal of the dead times due to gratings movement. In any potential future in-vivo application of grating interferometric tomography, shorter acquisition time will result in reduced motion artefacts. Additionally, the analysis of the signal-to-noise ratio (SNR) obtained in the reconstructed images suggests that the method may be more robust to noise than the phase stepping, and thus may allow reducing the delivered radiation dose. A more detailed study will be needed to thoroughly investigate this point.

It is noteworthy to remark the analogy between working within the linear region of the intensity function *G* in grating interferometry and acquiring images with the analyzer-based imaging technique [5,6] within the linear-slope region at approximately 50% the peak height of the rocking curve. The same signal linear dependence on absorption and refraction is also encountered within the "partial illumination condition" which is the basis of the "coded-aperture" imaging approach developed by Olivo et al. [8]. This implies that the proposed reconstruction technique is also applicable to images acquired using both the analyzer-based and the coded-aperture setups.

We demonstrated the feasibility of the method for both a simple test phantom and a complex biological sample. Furthermore, the results show not only a good quality of the reconstructed images, but also very good agreement with what predicted by theory. We therefore believe that the here-proposed method has the potential to find applications in many fields, in particular in possible future medical applications of X-ray grating interferometry, seen its advantages with respect to the usual phase stepping method.

Acknowledgements

We acknowledge the Laboratory for Micro- and Nanotechnology (Paul Scherrer Institut, Villigen, Switzerland) and the Institute for Microstructure Technology (Karlsruhe Institute of Technology, Germany) for providing the gratings used in this experiment. This work has been supported through the user program of the Karlsruhe Nano Micro Facility (KNMF). We also thank the Institute of Forensic Medicine of the Ludwig-Maximilians University (Munich, Germany) for providing the biological sample. The beamline staff of ID19 is acknowledged for their assistance in the preparation of the measurements. P.C. Diemoz, P. Coan, A. Bravin and C. Glaser acknowledge support through the DFG Cluster of Excellence Munich – Centre for Advanced Photonics.

#135564 - $15.00 USD Received 23 Sep 2010; revised 26 Oct 2010; accepted 27 Oct 2010; published 14 Jan 2011